HHS Public Access

Author manuscript

Mol Cancer Res. Author manuscript; available in PMC 2022 June 01.

Vulnerability of IDH1 mutant cancers to histone deacetylase inhibition via orthogonal suppression of DNA repair

Jonathan Dow[1,2], **Adam Krysztofiak**[1], **Yanfeng Liu**[1,2], **Daniel A. Colon-Rios**[1], **Faye A. Rogers**[1], **Peter M. Glazer**[1,2]

[1]Department of Therapeutic Radiology, Yale University School of Medicine. New Haven, Connecticut.

[2]Department of Genetics, Yale University School of Medicine. New Haven, Connecticut.

Abstract

Exploitation of DNA repair defects has enabled major advances in treating specific cancers. Recent work discovered that the oncometabolite 2-hydroxyglutarate (2-HG), produced by neomorphic isocitrate dehydrogenase 1/2 (IDH1/2) mutations, confers a homology directed repair (HDR) defect through 2-HG-induced histone hypermethylation masking HDR signaling. Here, we report that IDH1 mutant cancer cells are profoundly sensitive to the histone deacetylase inhibitor (HDACi) vorinostat, by further suppressing the residual HDR in 2-HG-producing cells. Vorinostat down-regulates repair factors BRCA1 and RAD51 via disrupted E2F-factor regulation, causing increased DNA double strand breaks, reduced DNA repair factor foci, and functional HDR deficiency even beyond 2-HG's effects. This results in greater cell death of IDH1 mutant cells and confers synergy with radiation and PARPi, both against cells in culture and patient-derived tumor xenografts. Our work identifies HDACi's utility against IDH1 mutant cancers, and presents IDH1/2 mutations as potential biomarkers to guide trials testing HDACi in gliomas and other malignancies.

Introduction

Recurrent metabolic gene mutations have been identified across various cancers, prompting the study of oncometabolites, metabolites whose accumulation is associated with cancer. Most notable are mutations in isocitrate dehydrogenase (IDH) genes, *IDH1* and *IDH2*, which convert isocitrate to α-ketoglutarate (α-KG). Cancer-associated IDH mutations occur as heterozygous missense mutations that confer the neomorphic function of converting α-KG to 2-hydroxyglutarate (2-HG) (1). IDH1/2 mutations are found in multiple cancers, including 80% of low-grade gliomas, 20% of higher-grade glioblastomas (2), 20% of acute myeloid leukemias (3) and 20% of cholangiocarcinomas (4).

Corresponding Author: Peter M. Glazer, Yale University, 15 York Street, HRT 140, P.O. Box 208040, New Haven, CT 06510-8040. Phone: 203-737-2788; Fax: 203-785-6309; peter.glazer@yale.edu.

Conflicts of interest:

P.M.G. is an inventor on the U.S. patent application no. 62/344,678 submitted by Yale University, which covers compositions and methods for targeting and treating HDR-deficient tumors.

2-HG's oncogenic role has been linked to its inhibition of α-KG-dependent dioxygenases, outcompeting α-KG due to similar chemical structure and highly elevated concentrations. These enzymes include the JmjC domain-containing histone demethylases (KDMs), whose inhibition is linked to 2-HG-induced histone hypermethylation (5). Investigation of epigenetic aberrations in 2-HG-producing cells' has largely focused on altered gene expression (6). Recent work presented a new dimension, identifying a DNA repair defect (7), consistent with improved survival of IDH mutant glioblastoma patients (8) and superior response to radiation and chemotherapy (9,10). An initial investigation of DNA repair in IDH1/2 mutant cells found a defect in homology directed repair (HDR), correlating with sensitivity to poly(ADP-ribose) polymerase inhibitors (PARPi) (11). PARPi vulnerability as a potential therapeutic strategy was first demonstrated in *BRCA1/2*-mutant cancers, capitalizing on HDR deficiency by inhibiting single-strand break repair (12,13). Mechanistic studies have revealed that IDH1/2 mutations impact HDR upstream from BRCA1/2 by disrupting early chromatin signaling at a double-strand break site. Specifically, histone demethylase KDM4B inhibition results in aberrant histone 3 lysine 9 trimethylation (H3K9me3) that masks an H3K9 methylation signal essential for HDR factor recruitment. However, this inhibition is not complete, as residual HDR can still be detected in IDH1 mutant cells at sites that remain hypomethylated despite elevated 2-HG levels (7). This prompted us to hypothesize that further suppression of HDR in IDH1 mutant cells by histone deacetylase inhibitors (HDACi) might present another mechanism for IDH mutant-specific targeting.

HDACi are known to inhibit HDR by down-regulating the expression of repair factors RAD51 and BRCA1 (14–18). These effects are reported for vorinostat, also known as SAHA, an FDA-approved HDACi that inhibits Class I and II HDACs and crosses the blood brain barrier (19,20). Targeting RAD51 and BRCA1 expression presents an attractive approach for suppressing residual HDR in IDH mutant cells, as reducing factor availability acts orthogonally to impaired recruitment. Additionally, HDACi are established radiosensitizers and synergize with PARPi in various cancer types (18,21–27). Based on pre-clinical studies against wild-type *IDH* gliomas, alone and in combination with PARPi and radiation (28–34), SAHA has been advanced into clinical trials for glioma (35). However, these trials were conducted without selection by IDH1/2 status and have yielded only modest results.

Here, we have sought to test SAHA's effect on the DNA repair and survival of IDH mutant cells and tumors, with the ultimate goal of informing future trials. We demonstrate SAHA's ability to down-regulate HDR factor expression, specifically through E2F-factor transcriptional regulation. Down-regulation of these factors further decreases the residual HDR in IDH1 mutant cells, as measured by reporter gene HDR assays, DNA repair factor foci formation and DNA DSB levels via the comet assay. This HDR suppression mediates single-agent activity of SAHA against IDH1 mutant cells and provides for enhanced effectiveness of SAHA in combination with radiation or PARPi, yielding marked tumor growth delay in patient-derived, IDH1 mutant human xenografts in mice. These findings identify SAHA as a potential agent for specific targeting of IDH1/2 mutant cancers.

Materials and Methods

Cell Culture

HT1080, U2OS EJDR, maintained in DMEM+10% FBS, HCT116 *IDH1* +/+ and *IDH1* R132H/+, maintained in McCoy's 5A+10% FBS, and U87 *IDH1* +/+ and *IDH1* R132H/+, maintained in DMEM/F12+10% FBS, were obtained from R. Bindra (Yale University School of Medicine). Immortalized astrocytes were obtained from T. Chan (Cleveland Clinic) (36) and maintained in DMEM+10% FBS. Cells were passaged twice after thawing before use in experiments, regularly tested for mycoplasma (MycoAlert, Lonza) and authenticated using short tandem repeat profiling (ATCC).

Drugs and reagents

SAHA, olaparib, BMN-673, AGI-5198 and temozolomide were all obtained from SelleckChem, and dissolved in DMSO for cell culture experiments. For animal tumor studies, BMN-673 was diluted in a vehicle containing 10% dimethylacetamide, 6% Kolliphor HS 15 and 84% PBS. SAHA was diluted in PBS. Both were administered to mice via oral gavage five days a week, for three weeks. Octyl-2-HG ((2R)-octyl-alpha-hydroxyglutarate) (Cayman Chemical) and Octyl-α-KG (Sigma-Aldrich) were dissolved in DMSO. Horizon Dharmacon ON-TARGETplus Human BRCA1 and RAD51 siRNA were used at 20 nM for 72 hours.

Western blotting

Cells were lysed in AZ lysis buffer. Band intensity was quantified by densitometry via ImageJ software, and normalized to Vinculin or β Actin as endogenous controls. Antibodies are provided in Supplementary Materials.

RTqPCR analysis

RNA was isolated via RNA Miniprep kit (Qiagen) and used for cDNA synthesis via High-Capacity cDNA Reverse Transcription Kit (Applied Biosystems). cDNA was used in RTqPCR assays using Taqman Universal PCR Master Mix and Gene Expression Assays (Applied Biosystems) and a StepOnePlus RT-PCR system (Thermo Fisher Scientific). *18S* was used as an endogenous control.

EJDR HDR assay

U2OS EJDR cells were pretreated with SAHA for 24 hours and 2-HG for 3 days before adding ligands, triamcinolone (0.5 μM, Sigma) and Shield1 (100 nM, Clontech), to media for 24 hours. Cells were analyzed by flow cytometry after 72 hours for GFP signal.

Neutral comet assays

Neutral comet assays were performed as previously described (11). Imaging was completed with an EVOS FL microscope (Advanced Microscopy Group) and analyzed via OpenComet software (37).

Immunofluorescent foci analysis

Cells were seeded in 8-chamber slides, with or without SAHA, and irradiated 24 hours later using an X-RAD 320 X-Ray Biological Irradiator (Precision X-Ray Inc). Non-irradiated controls were completed in parallel. Cells were fixed, permeabilized and incubated in blocking buffer overnight at 4 C. Cells were incubated in RAD51 primary for 30 minutes at RT, and overnight at 4 C. After washes, samples were incubated with secondary in blocking for 75 min at RT. After washes, samples were incubated with γ-H2AX primary for 90 minutes at RT, and overnight at 4 C. Antibodies are provided in Supplementary Materials. DNA was stained with DAPI for 15 minutes at RT. After washes, chambers were removed and slides were covered with coverslips using DAKO Fluorescence Mounting Medium (Dako NA Inc.) and sealed with nail polish. Images were taken using a Nikon Eclipse TiE inverted fluorescence microscope (Nikon Corporation), Plan Apo 60X/1.40 Oil DIC h objective, CSU-W1 confocal spinning disk unit (Yokogawa Corporation of America) with the iXon Ultra888 EMCCD (Andor Technology), MLC 400B laser unit (Agilent Technologies) and NIS Elements 4.30 software (Nikon Corporation). Images were saved as multi-channel .nd2 files with no further editing. Representative images of 55 × 55 microns were prepared with ImageJ software and saved as 8-bit .tiff images. For γ-H2AX and RAD51, cells with greater than 10 foci/nuclei were considered foci-positive.

Cell viability and clonogenic assays

Cell viability assays were performed using CellTiter-Glo (Promega). 1000 cells/well were seeded in a 96-well plate, then treated with SAHA, olaparib or BMN-673 for 7 days. Luminescence was quantified using a Synergy HR plate reader (BioTek). 500 cells/well were seeded in 6-well plates in drug free media for clonogenic survival assays, then changed to drugged medium or irradiated after 24 hours. Cells were treated with SAHA for 2 days, olaparib, BMN-673 and Temozolomide for 5 days. Plates were kept in an incubator for 10–14 days, depending on colony size. Cells were washed in PBS, stained with crystal violet, and manually counted. For combinations, cells were seeded into SAHA-drugged media, then irradiated or switched to combined treatment after 24 hours. Synergy was calculated via Combenefit software's HSA model (38).

Mouse tumor xenograft studies

Human HT1080 cells (5×10^6) and HCT116 cells (1×10^6) were implanted subcutaneously in the flanks of athymic nu/nu mice (Harlan). Three times a week, tumors were measured using calipers to calculate tumor volume [$V = ½(4\pi/3)(\text{length}/2)(\text{width}/2)(\text{height})$]. Protocol was approved by Yale University Institutional Animal Care and Use Committee.

Statistical analysis

Statistical analysis was completed in GraphPad Prism. Unless otherwise stated, data is presented as means ± SEM and n = 3 replicates. Significance was determined using unpaired t tests or ANOVA, all two-sided with a testing level of 0.05.

Results

SAHA suppresses HDR factor expression in IDH1 mutant cells

To first assess SAHA's impact on DNA repair in IDH1 mutant cells, we tested changes in the expression of repair factors BRCA1 and RAD51 after treatment with SAHA. We chose the HT1080 line, a fibrosarcoma line carrying an endogenous *IDH1* R132C/+ mutation, as well as an engineered U87 isogenic glioma pair, mutant *IDH1* R132H/+ and wild-type *IDH1* +/+. We observed dose-dependent decreases in BRCA1 and RAD51 protein, to greater effect in the U87 glioma cell background, and even greater decreases in respective mRNA levels (Fig. 1A and B). We also probed SAHA's epigenetic effect on IDH1 mutant cells, looking at histone 3 lysine 9 trimethylation (H3K9me3) for 2-HG-induced hypermethylation as well as H3K9 acetylation (H3K9ac) and pan histone 4 acetylation (H4ac) for HDACi effects. We observed similarly elevated acetylation in all three lines, while seeing larger decreases in H3K9me3 in IDH1 mutant cells, due to elevated baselines (Supplementary Fig. 1A). These results reveal that SAHA reduces 2-HG-induced hypermethylation, while suppressing HDR factor expression, informing our study of DNA repair function.

Additionally, we investigated whether SAHA's suppression of HDR factor expression was sustained during a radiation-induced DNA damage response, in patient-derived HT1080 cells. Radiation induced a time-dependent increase in BRCA1 and RAD51 in control DMSO-treated HT1080 cells, whereas there was a sustained down-regulation of BRCA1 and RAD51 in SAHA-treated cells, even after radiation (Fig. 1C).

SAHA-induced HDR down-regulation is mediated via E2F1 loss

Seeing strong suppression of RAD51 and BRCA1 expression at the mRNA level by SAHA treatment, we sought to identify the mechanism of the transcriptional down-regulation. It has been proposed that HDACi HDR suppression may be due to disrupted E2F transcription factor regulation, specifically E2F1 activator loss, in prostate cancer models (16). E2F-factor dysregulation is also more broadly established as an HDR suppression mechanism in hypoxia and specific drug treatments (39–42). Hence, we first tested SAHA's effect on E2F1 activator and E2F4 repressor expression, in both HT1080 and U87 matched pair cells. SAHA decreased both E2F1 and E2F4 protein and mRNA expression, but with greater impact on E2F1 (Fig. 2A and B). This differential effect prompted us to perform chromatin immuno-precipitation (ChIP) assays for the two factors to interrogate occupancy at *RAD51* and *BRCA1* promoter sites, with and without treatment, in HT1080 and U87 matched pair cells. E2F1 and E2F4 ChIP revealed occupancy decreases in both factors but, importantly, there was a much greater fold decrease in E2F1 activator occupancy, as previously reported (16) (Fig. 2C). This large reduction in E2F1 occupancy at *RAD51* and *BRCA1*'s promoter sites provides a mechanistic explanation for their transcriptional down-regulation.

SAHA suppresses residual HDR in IDH1 mutant cells

After confirming that SAHA down-regulates HDR factor expression, we next investigated whether this has a functional effect on DNA repair in IDH1 mutant cells. Because of SAHA's ability to decrease H3K9me3 levels by enhancing H3K9ac, we were concerned that this might mitigate 2-HG's effects on DNA repair, which result from H3K9

hypermethylation. To address this, we tested whether intermediate 2-HG and SAHA doses, that alone cause moderate reductions in HDR, might worsen DNA repair in the HDR pathway in combination. We used the U2OS EJDR reporter cell line, a human osteosarcoma cell line that carries a ligand-inducible, chromosomally integrated green fluorescent protein (GFP)-based HDR reporter (43). This system employs a widely used approach for gauging HDR activity: restoration of a mutated GFP reporter when a neighboring donor region is used as a repair template due to sequence homology. Repair is triggered by site-specific cutting within the reporter gene by a ligand-responsive I-SceI nuclease, following the addition of the ligands shield-1 and triamcinolone which enable protein stabilization and nuclear localization. U2OS EJDR cells were pretreated with SAHA and/or cell-permeable (2R)-Octyl-2-HG (here-on referred as Octyl-2-HG) before ligand treatment and scored for HDR by quantifying GFP positivity. By itself, Octyl-2-HG treatment elevated H3K9me3 levels and decreased HDR activity, as expected (11). Octyl-2-HG's suppression of HDR activity was dose-dependent, with a moderate effect seen with 0.5 mM and a larger decrease with 1 mM. This decrease in HDR treatment is specific to Octyl-2-HG, as no significant reduction was seen when cells were treated with a high dose of Octyl-α-KG. SAHA treatment alone decreased HDR, also in a dose-dependent manner, as well as down-regulating BRCA1 and RAD51 expression while increasing H3K9ac. High Octyl-2-HG and SAHA doses lead to significant HDR suppression, though not to the extent of full siRNA knockdown of RAD51 and BRCA1. Importantly, we found that the combination of moderate Octyl-2-HG and SAHA doses had an additive effect in suppressing HDR, resulting in a reduction similar to high single-agent doses. This result demonstrates that SAHA worsens the overall DNA repair deficiency in cells with high 2-HG (although by a different mechanism) and does not reverse it (Fig. 3A and B). Notably, addition of SAHA overrode Octyl-2-HG treatment's increase in histone hypermethylation, seen at H3 lysines 9, 27 and 36, with HDACi forcing robust global acetylation seen via western blot (Fig. 3B, Supplementary Fig. 2A). 2-HG intracellular concentrations were confirmed by a 2HGDH-mediated enzyme assay after treatment (Supplementary Fig. 2B), and siRNA knockdown of BRCA1 and RAD51 was confirmed by western blot analysis (Supplementary Fig. 2C). The additive effect of combined SAHA and Octyl-2-HG treatment in suppressing HDR shows that SAHA's effect of increasing H3K9 acetylation while decreasing methylation is not sufficient to reverse the HDR defect caused by 2-HG.

Next, we directly assessed DNA DSB levels in IDH1 mutant cells treated with or without SAHA by measuring DSBs using the neutral comet assay. In patient-derived HT1080 *IDH1* R132C/+ cells, SAHA treatment elevated the comet phenotype, suggesting increased DNA damage in the form of DSBs (Fig. 3C). To test the relative contribution of 2-HG on SAHA treatment's effect, HT1080 cells were treated with AGI-5198, an inhibitor of IDH1 R132C's neomorphic 2-HG production (44), with or without SAHA. As expected, AGI-5198 significantly reduced the comet phenotype (11), demonstrating 2-HG's role in increased DNA damage at baseline. With AGI-5198 treatment, SAHA still elevated the level of DSB damage from this lower baseline (Fig. 3C). SAHA's effect of increasing DSBs was also seen in both the IDH1 wild-type and matched IDH1 R132H/+ U87 cells, with IDH1 mutant cells having increased DSB damage at baseline (Fig. 3D, Supplementary Fig. 3A). These results demonstrate that SAHA's repair effect occurs independent of 2-HG

production, and is additive in IDH1 mutant cells, causing greater DNA damage. Next, we tested the impact on DNA DSBs when SAHA is combined with the PARPi olaparib. We found that olaparib increased the comet tail moments in HT1080 cells, with and without AGI-5198 treatment, and in the U87 pair, relative to baseline, in keeping with prior work (11). Importantly, we found that combination with SAHA increased the level of DSBs above and beyond the effect of olaparib alone (Fig. 3C and D, Supplementary Fig. 3A). IDH1 mutant U87 cells ultimately experienced higher levels of cellular DNA damage following SAHA treatment, likely resulting from their baseline repair deficiency. This differential effect was also seen with treatment of siBRCA1 and siRAD51, correlating with the impact of HDR downregulation caused by SAHA. HDR factor loss via siRNA knockdown elevated wildtype U87 cells to the mutant baseline and IDH1 mutant cells to a much higher level of cellular DNA damage (Supplementary Fig. 3B and C). These results demonstrate that SAHA elevates constitutive DSBs to greater effect in IDH1 mutant cells and presents a rational for possible combination with PARPi.

Lastly, to further test the functional HDR effect caused by SAHA, we performed immunofluorescent DNA repair factor foci analyses for RAD51 (indicative of HDR) and γ-H2AX (a marker for DSBs) post irradiation in HT1080 and the U87 pair. Specifically, cells were scored foci-positive with a count of ten or more foci per nucleus. Across the three cell lines, SAHA treatment decreased RAD51 foci at time-points both before and after radiation, indicative of reduced HDR capacity, consistent with the gene expression and comet assay data (Fig. 3E and G, Supplementary Fig. 4A). We did note more diffuse staining and greater background in SAHA-treated cells, potentially resulting from reduced RAD51 abundance and reduced signal-to-noise. In accord with reduced RAD51 foci, increased γ-H2AX foci formation post-radiation persisted at higher levels and for longer times over 24 hours in the SAHA-treated cells, indicating unresolved DSBs (Fig. 3F and G, Supplementary Fig. 4A). SAHA-treated cells had both more and larger γ-H2AX foci than untreated cells, as seen in representative images, potentially indicative of more complex DSB sites (Fig. 3G, Supplementary Fig. 4A). Foci formation patterns of the matched U87 glioma pair demonstrates the expected DNA repair defect in IDH1 mutant cells, with greater damage measured by γ-H2AX foci and reduced HDR measured by RAD51 foci. SAHA's effects, while seen in both IDH1 wild-type and mutant U87 glioma cells, ultimately results in a greater repair crisis in IDH1 mutant cells.

IDH1 mutant cells have a greater vulnerability to SAHA treatment

To test the implication of this SAHA-induced repair crisis on cell survival, we investigated whether IDH1 mutant cells have a greater sensitivity to SAHA treatment. Using the U87 pair, we performed long-term clonogenic survival assays (CSA) and short-term adenosine 5′-triphosphate (ATP)–based viability assays following SAHA treatment. We saw greater SAHA sensitivity in IDH1 mutant glioma cells with both methods (Fig. 4A), to an extent similar to the sensitivity seen via CSA of glioma cells treated with the PARPi olaparib and BMN-673 (talazoparib) (Supplementary Fig. 5A). IDH1 mutant sensitivity was further supported by a greater increase of cleaved PARP, an established apoptosis marker. The mutant U87 line experienced a greater than 10-fold increase in cleaved PARP from baseline following SAHA treatment versus a 2.4-fold increase in wild-type (Fig. 4B).

To further demonstrate IDH1 mutant cells' heightened vulnerability to SAHA, we utilized an immortalized human astrocyte line with a stably integrated, doxycycline(dox)-inducible IDH1 R132H expression construct. Astrocytes were treated with or without dox for multiple passages, then tested for SAHA sensitivity. As seen in the U87 matched pair, mutant IDH1-expressing astrocytes had greater SAHA sensitivity (Fig. 4C), similar in extent to their sensitivity to olaparib and BMN-673 (Supplementary Fig. 5B). SAHA treatment also resulted in greater DNA damage as measured via the comet assay in the dox-induced astrocytes, consistent with the cell survival and viability data (Supplementary Fig. 3D). Furthermore, there was a 5.0-fold increase in cleaved PARP response in dox-induced cells versus 1.3-fold in the uninduced cells, while BRCA1 and RAD51 suppression was comparable in both contexts (Fig. 4D). These results further demonstrate SAHA's strong effect against IDH1 mutant cells.

SAHA combination with radiation and PARPi has greater effects against IDH1 mutant cells

Next, we sought to identify combinations that capitalized on this HDR suppression, first investigating SAHA's combination with radiation against IDH1 mutant cells via CSAs in HT1080 and U87 matched pair cells. Combination of SAHA and radiation treatment caused an additive effect across all three lines, but this combined effect was greater in IDH1 mutant cells (U87 +/+ $P = 0.1836$, U87 R132H/+ $P < 0.001$) (Fig. 5A). HSA model synergy of this combination showed a synergistic effect across all three lines, though to a much greater degree in IDH1 mutant HT1080 (R132C) and U87 (R132H) cells (Supplementary Fig. 6A). The sensitivity of the IDH1 mutant U87 glioma line to this combination is particularly significant given the modest results reported from clinical trials of SAHA in glioma that were conducted without IDH1/2 status selection, specifically, those of a Phase I/II study (NCT00731731) testing combination of SAHA, radiation and temozolomide (TMZ) (45). Pertinent to this, we also tested the combination of SAHA and TMZ in the U87 matched pair. We found increased TMZ sensitivity in the IDH1 mutant cells, as expected (46), as well as a stronger synergistic effect in combination with SAHA (Fig. 5B, Supplementary Fig 6B). These results present a further rationale for using IDH1/2 mutations as biomarkers for future clinical trials testing HDACi in combination therapies in patients with gliomas.

Next, given IDH1 mutant cells' strong PARPi sensitivity and SAHA's HDR suppression, we tested SAHA in combination with olaparib and BMN-673, in HT1080 and U87 matched pair cells. We found very strong combined effects with both olaparib and BMN-673 in all three lines, though survival of the IDH1 mutant cells was more highly affected (Fig. 5C). The PARPi plus SAHA combination had strong synergy, as expected, in both IDH1 mutant and wild-type U87 lines, though importantly IDH1 mutant cells showed greater cell death (Supplementary Fig. 6C and D).

To extend our findings to an in vivo model, we performed a tumor xenograft study in mice using HT1080 cells, with four arms testing vehicle, SAHA alone, BMN-673 alone, and SAHA plus BMN-673 combination. Interestingly, moderate SAHA dosing strongly delayed tumor growth of the IDH1 mutant HT1080 xenografts, with a greater growth inhibition than seen with aggressive BMN-673 dosing. SAHA's effect was further enhanced in combination with BMN-673, yielding the greatest tumor growth delay (Fig. 5D). There was no added

toxicity in the combination treatment arm beyond single-agent effects as measured by mouse body weight throughout the study and bone marrow cell counts at the study's end (Fig. 5E and F).

We replicated these results with a second tumor xenograft model using an engineered *IDH1* R132H/+ HCT116 colorectal carcinoma line. In cell culture, SAHA had the same effects on HCT116 cells as seen in glioma and patient-derived cells: downregulation of BRCA1 and RAD51 expression (Supplementary Fig. 7A), increased constitutive DSBs measured via neutral comet assay (Supplementary Fig. 7B), and stronger effects alone and in combination with PARPi against IDH1 mutant cells (Supplementary Fig. 7C and D). PARPi plus SAHA combination had strong synergy in both IDH1 mutant and wild-type cells (Supplementary Fig. 7E). This synergy was demonstrated in mutant IDH1 HCT116 tumor xenografts, with SAHA plus BMN-673 combination resulting in the greatest tumor growth delay (Fig. 5G). These results strongly demonstrate the benefit of SAHA plus PARPi combination against IDH1 mutant tumors in vivo, highlighting HDACi's potential clinical utility in the context of IDH mutant malignancies.

Discussion

In this work, we demonstrate the HDACi SAHA's ability to suppress residual HDR in IDH1 mutant cells, through down-regulation of repair factors BRCA1 and RAD51 mediated by disrupted E2F-factor transcriptional regulation. This mechanism occurs independent of 2-HG, and displays an additive effect resulting in a greater DNA repair crisis due to compounding losses in DNA repair factor abundance and DNA repair signaling. This repair crisis underlies SAHA's strong effects against IDH1 mutant cells alone and in combination with radiation and PARPi. We demonstrate the effectiveness of SAHA alone and in combination with PARPi BMN-673 against patient-derived, IDH1 mutant HT1080 mouse tumor xenografts. The benefit of HDACi use in fibrosarcoma was previously identified with a large SAHA dose (1050 mg/kg/week) against HT1080 xenografts, though without exploring the role of IDH1 mutant status or DNA repair (47). Here, we present strong tumor growth delay with much smaller dosing (150 mg/kg/week), and data demonstrating SAHA's suppression of residual HDR in IDH1 mutant cells.

HDACi's effects on HDR factor expression (14–18) and its utility against wild-type gliomas (31–34) has been previously explored, but not in the IDH1/2 mutant context. Our work provides new insight into the utility of HDACi in the subset of gliomas that are IDH1/2 mutant, demonstrating HDACi suppression of residual HDR, based on reporter gene HDR assays and repair foci analyses. A remaining question is the extent to which elevated H3K9ac as a result of HDAC inhibition may impede methylation-based epigenetic signaling and factor recruitment at a DSB, which we plan to address in future studies as another potential mechanistic contribution. Nonetheless, our focus in this work centered on SAHA's functional impact on IDH1 mutant cells' residual HDR, and its resulting therapeutic utility.

We further present multiple treatment combinations that capitalize on the DNA repair crisis in IDH1 mutant cells following SAHA treatment. SAHA's IDH1 mutant-dependent synergy with radiation and TMZ, seen in glioma cells, provides clear support for consideration

of IDH1/2 status in the design of clinical trials using these agents. Furthermore, the effectiveness of the SAHA plus PARPi combination was demonstrated in vivo against two IDH1 mutant xenograft models, presenting support for testing this strategy in trials of PARPi in IDH1/2 mutant cancers. SAHA's utility against IDH1 mutant cells, alone or in combination, has major relevance to glioma, though the application of PARPi and SAHA will depend on the advancement of suitable brain penetrant PARPi for clinical use. Overall, the work presented here highlights a new strategy for targeting IDH1/2 mutant cancers based on suppression of residual HDR with HDACi.

Supplementary Material

Refer to Web version on PubMed Central for supplementary material.

Acknowledgments:

This work was supported by the NIH grants R35CA197574 and R01ES005775 to P. M. Glazer. J. Dow was supported by the National Institute of General Medical Science training grant T32GM007499. We thank D. Hegan and A. Dhawan for their assistance. We thank Dr. Joerg Nikolaus from the Yale West Campus Imaging Core for technical support.

References:

1. Dang L, White DW, Gross S, Bennett BD, Bittinger MA, Driggers EM, et al. Cancer-associated IDH1 mutations produce 2-hydroxyglutarate. Nature 2009;462:739–44 [PubMed: 19935646]
2. Yan H, Parsons DW, Jin G, McLendon R, Rasheed BA, Yuan W, et al. IDH1 and IDH2 Mutations in Gliomas. New England Journal of Medicine 2009;360:765–73
3. Mardis ER, Ding L, Dooling DJ, Larson DE, McLellan MD, Chen K, et al. Recurring Mutations Found by Sequencing an Acute Myeloid Leukemia Genome. New England Journal of Medicine 2009;361:1058–66
4. Jiao Y, Pawlik TM, Anders RA, Selaru FM, Streppel MM, Lucas DJ, et al. Exome sequencing identifies frequent inactivating mutations in BAP1, ARID1A and PBRM1 in intrahepatic cholangiocarcinomas. Nature Genetics 2013;45:1470–3 [PubMed: 24185509]
5. Xu W, Yang H, Liu Y, Yang Y, Wang P, Kim S-H, et al. Oncometabolite 2-Hydroxyglutarate Is a Competitive Inhibitor of α-Ketoglutarate-Dependent Dioxygenases. Cancer Cell 2011;19:17–30 [PubMed: 21251613]
6. Losman JA, Kaelin WG Jr. What a difference a hydroxyl makes: mutant IDH, (R)-2-hydroxyglutarate, and cancer. Genes Dev 2013;27:836–52 [PubMed: 23630074]
7. Sulkowski PL, Oeck S, Dow J, Economos NG, Mirfakhraie L, Liu Y, et al. Oncometabolites suppress DNA repair by disrupting local chromatin signalling. Nature 2020;582:586–91 [PubMed: 32494005]
8. Parsons DW, Jones S, Zhang X, Lin JC-H, Leary RJ, Angenendt P, et al. An Integrated Genomic Analysis of Human Glioblastoma Multiforme. Science 2008;321:1807–12 [PubMed: 18772396]
9. Tran AN, Lai A, Li S, Pope WB, Teixeira S, Harris RJ, et al. Increased sensitivity to radiochemotherapy in IDH1 mutant glioblastoma as demonstrated by serial quantitative MR volumetry. Neuro-Oncology 2014;16:414–20 [PubMed: 24305712]
10. Cairncross JG, Wang M, Jenkins RB, Shaw EG, Giannini C, Brachman DG, et al. Benefit From Procarbazine, Lomustine, and Vincristine in Oligodendroglial Tumors Is Associated With Mutation of IDH. Journal of Clinical Oncology 2014;32:783–90 [PubMed: 24516018]
11. Sulkowski PL, Corso CD, Robinson ND, Scanlon SE, Purshouse KR, Bai H, et al. 2-Hydroxyglutarate produced by neomorphic IDH mutations suppresses homologous recombination and induces PARP inhibitor sensitivity. Science Translational Medicine 2017;9:eaal2463 [PubMed: 28148839]

12. Bryant HE, Schultz N, Thomas HD, Parker KM, Flower D, Lopez E, et al. Specific killing of BRCA2-deficient tumours with inhibitors of poly(ADP-ribose) polymerase. Nature 2005;434:913–7 [PubMed: 15829966]
13. Farmer H, McCabe N, Lord CJ, Tutt AN, Johnson DA, Richardson TB, et al. Targeting the DNA repair defect in BRCA mutant cells as a therapeutic strategy. Nature 2005;434:917–21 [PubMed: 15829967]
14. Adimoolam S, Sirisawad M, Chen J, Thiemann P, Ford JM, Buggy JJ. HDAC inhibitor PCI-24781 decreases RAD51 expression and inhibits homologous recombination. Proceedings of the National Academy of Sciences 2007;104:19482–7
15. Weberpals JI, O'Brien AM, Niknejad N, Garbuio KD, Clark-Knowles KV, Dimitroulakos J. The effect of the histone deacetylase inhibitor M344 on BRCA1 expression in breast and ovarian cancer cells. Cancer Cell International 2011;11:29 [PubMed: 21854619]
16. Kachhap SK, Rosmus N, Collis SJ, Kortenhorst MS, Wissing MD, Hedayati M, et al. Downregulation of homologous recombination DNA repair genes by HDAC inhibition in prostate cancer is mediated through the E2F1 transcription factor. PLoS One 2010;5:e11208 [PubMed: 20585447]
17. Lai T-H, Ewald B, Zecevic A, Liu C, Sulda M, Papaioannou D, et al. HDAC Inhibition Induces MicroRNA-182, which Targets RAD51 and Impairs HR Repair to Sensitize Cells to Sapacitabine in Acute Myelogenous Leukemia. Clinical Cancer Research 2016;22:3537–49 [PubMed: 26858310]
18. Ha K, Fiskus W, Choi DS, Bhaskara S, Cerchietti L, Devaraj SGT, et al. Histone deacetylase inhibitor treatment induces 'BRCAness' and synergistic lethality with PARP inhibitor and cisplatin against human triple negative breast cancer cells. Oncotarget 2014;5:5637–50 [PubMed: 25026298]
19. Villar-Garea A, Esteller M. Histone deacetylase inhibitors: understanding a new wave of anticancer agents. Int J Cancer 2004;112:171–8 [PubMed: 15352027]
20. Palmieri D, Lockman PR, Thomas FC, Hua E, Herring J, Hargrave E, et al. Vorinostat Inhibits Brain Metastatic Colonization in a Model of Triple-Negative Breast Cancer and Induces DNA Double-Strand Breaks. Clinical Cancer Research 2009;15:6148–57 [PubMed: 19789319]
21. Munshi A, Tanaka T, Hobbs ML, Tucker SL, Richon VM, Meyn RE. Vorinostat, a histone deacetylase inhibitor, enhances the response of human tumor cells to ionizing radiation through prolongation of gamma-H2AX foci. Mol Cancer Ther 2006;5:1967–74 [PubMed: 16928817]
22. Chen X, Wong JY, Wong P, Radany EH. Low-dose valproic acid enhances radiosensitivity of prostate cancer through acetylated p53-dependent modulation of mitochondrial membrane potential and apoptosis. Mol Cancer Res 2011;9:448–61 [PubMed: 21303901]
23. Chen X, Wong P, Radany EH, Stark JM, Laulier C, Wong JYC. Suberoylanilide Hydroxamic Acid as a Radiosensitizer through Modulation of RAD51 Protein and Inhibition of Homology-Directed Repair in Multiple Myeloma. Molecular Cancer Research 2012;10:1052–64 [PubMed: 22729783]
24. Min A, Im SA, Kim DK, Song SH, Kim HJ, Lee KH, et al. Histone deacetylase inhibitor, suberoylanilide hydroxamic acid (SAHA), enhances anti-tumor effects of the poly (ADP-ribose) polymerase (PARP) inhibitor olaparib in triple-negative breast cancer cells. Breast Cancer Res 2015;17:33 [PubMed: 25888415]
25. Konstantinopoulos PA, Wilson AJ, Saskowski J, Wass E, Khabele D. Suberoylanilide hydroxamic acid (SAHA) enhances olaparib activity by targeting homologous recombination DNA repair in ovarian cancer. Gynecol Oncol 2014;133:599–606 [PubMed: 24631446]
26. Chao OS, Goodman OB, Jr. Synergistic loss of prostate cancer cell viability by coinhibition of HDAC and PARP. Mol Cancer Res 2014;12:1755–66 [PubMed: 25127709]
27. Yin L, Liu Y, Peng Y, Peng Y, Yu X, Gao Y, et al. PARP inhibitor veliparib and HDAC inhibitor SAHA synergistically co-target the UHRF1/BRCA1 DNA damage repair complex in prostate cancer cells. Journal of Experimental & Clinical Cancer Research 2018;37:153 [PubMed: 30012171]
28. Eyüpoglu IY, Hahnen E, Buslei R, Siebzehnrübl FA, Savaskan NE, Lüders M, et al. Suberoylanilide hydroxamic acid (SAHA) has potent anti-glioma properties in vitro, ex vivo and in vivo. J Neurochem 2005;93:992–9 [PubMed: 15857402]

29. Yin D, Ong JM, Hu J, Desmond JC, Kawamata N, Konda BM, et al. Suberoylanilide hydroxamic acid, a histone deacetylase inhibitor: effects on gene expression and growth of glioma cells in vitro and in vivo. Clin Cancer Res 2007;13:1045–52 [PubMed: 17289901]
30. Cornago M, Garcia-Alberich C, Blasco-Angulo N, Vall-Llaura N, Nager M, Herreros J, et al. Histone deacetylase inhibitors promote glioma cell death by G2 checkpoint abrogation leading to mitotic catastrophe. Cell Death Dis 2014;5:e1435 [PubMed: 25275596]
31. Hsu C-C, Chang W-C, Hsu T-I, Liu J-J, Yeh S-H, Wang J-Y, et al. Suberoylanilide hydroxamic acid represses glioma stem-like cells. Journal of Biomedical Science 2016;23:81 [PubMed: 27863490]
32. Yang X-F, Zhao Z-J, Liu J-J, Yang X-H, Gao Y, Zhao S, et al. SAHA and/or MG132 reverse the aggressive phenotypes of glioma cells: An in vitro and vivo study. Oncotarget 2017;8:3156–69 [PubMed: 27911270]
33. Barazzuol L, Jeynes JC, Merchant MJ, Wéra AC, Barry MA, Kirkby KJ, et al. Radiosensitization of glioblastoma cells using a histone deacetylase inhibitor (SAHA) comparing carbon ions with X-rays. Int J Radiat Biol 2015;91:90–8 [PubMed: 25040548]
34. Rasmussen RD, Gajjar MK, Jensen KE, Hamerlik P. Enhanced efficacy of combined HDAC and PARP targeting in glioblastoma. Mol Oncol 2016;10:751–63 [PubMed: 26794465]
35. Chen R, Zhang M, Zhou Y, Guo W, Yi M, Zhang Z, et al. The application of histone deacetylases inhibitors in glioblastoma. Journal of Experimental & Clinical Cancer Research 2020;39:138 [PubMed: 32682428]
36. Turcan S, Rohle D, Goenka A, Walsh LA, Fang F, Yilmaz E, et al. IDH1 mutation is sufficient to establish the glioma hypermethylator phenotype. Nature 2012;483:479–83 [PubMed: 22343889]
37. Gyori BM, Venkatachalam G, Thiagarajan PS, Hsu D, Clement MV. OpenComet: an automated tool for comet assay image analysis. Redox Biol 2014;2:457–65 [PubMed: 24624335]
38. Di Veroli GY, Fornari C, Wang D, Mollard S, Bramhall JL, Richards FM, et al. Combenefit: an interactive platform for the analysis and visualization of drug combinations. Bioinformatics 2016;32:2866–8 [PubMed: 27153664]
39. Bindra RS, Gibson SL, Meng A, Westermark U, Jasin M, Pierce AJ, et al. Hypoxia-induced down-regulation of BRCA1 expression by E2Fs. Cancer Res 2005;65:11597–604 [PubMed: 16357170]
40. Hegan DC, Lu Y, Stachelek GC, Crosby ME, Bindra RS, Glazer PM. Inhibition of poly(ADP-ribose) polymerase down-regulates BRCA1 and RAD51 in a pathway mediated by E2F4 and p130. Proc Natl Acad Sci U S A 2010;107:2201–6 [PubMed: 20133863]
41. Bindra RS, Glazer PM. Repression of RAD51 gene expression by E2F4/p130 complexes in hypoxia. Oncogene 2007;26:2048–57 [PubMed: 17001309]
42. Kaplan AR, Gueble SE, Liu Y, Oeck S, Kim H, Yun Z, et al. Cediranib suppresses homology-directed DNA repair through down-regulation of BRCA1/2 and RAD51. Sci Transl Med 2019;11
43. Bindra RS, Goglia AG, Jasin M, Powell SN. Development of an assay to measure mutagenic non-homologous end-joining repair activity in mammalian cells. Nucleic Acids Res 2013;41:e115 [PubMed: 23585275]
44. Li L, Paz AC, Wilky BA, Johnson B, Galoian K, Rosenberg A, et al. Treatment with a Small Molecule Mutant IDH1 Inhibitor Suppresses Tumorigenic Activity and Decreases Production of the Oncometabolite 2-Hydroxyglutarate in Human Chondrosarcoma Cells. PLoS One 2015;10:e0133813 [PubMed: 26368816]
45. Galanis E, Anderson SK, Miller CR, Sarkaria JN, Jaeckle K, Buckner JC, et al. Phase I/II trial of vorinostat combined with temozolomide and radiation therapy for newly diagnosed glioblastoma: results of Alliance N0874/ABTC 02. Neuro Oncol 2018;20:546–56 [PubMed: 29016887]
46. Lu Y, Kwintkiewicz J, Liu Y, Tech K, Frady LN, Su YT, et al. Chemosensitivity of IDH1-Mutated Gliomas Due to an Impairment in PARP1-Mediated DNA Repair. Cancer Res 2017;77:1709–18 [PubMed: 28202508]
47. Sampson ER, Amin V, Schwarz EM, O'Keefe RJ, Rosier RN. The histone deacetylase inhibitor vorinostat selectively sensitizes fibrosarcoma cells to chemotherapy. J Orthop Res 2011;29:623–32 [PubMed: 20957741]

Implications:

IDH1 mutant cells show profound vulnerability to HDACi treatment, alone and with PARPi and radiation, via HDR suppression, presenting IDH1/2 mutations as biomarkers for HDACi's use in gliomas and other malignancies.

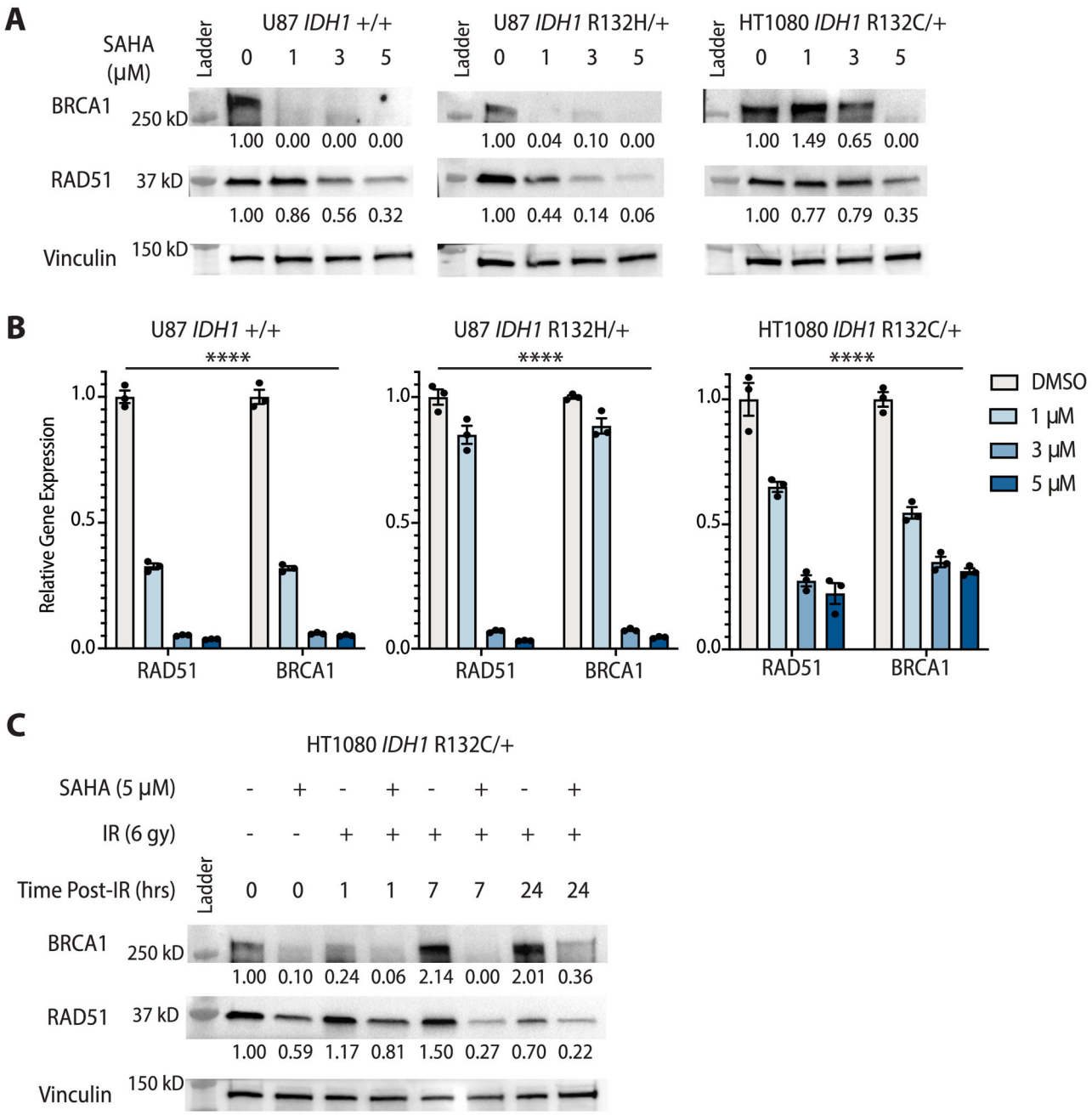

Figure 1: SAHA down-regulates HDR factor expression in IDH1 mutant cells

A, Western blot of HDR factors in glioma pair (U87) and patient-derived mutant IDH1 fibrosarcoma cells (HT1080) 24 hours after treatment with increasing SAHA doses (n = 3 independent experiments). **B**, Relative gene expression of HDR factors measured at the mRNA level by RTqPCR in U87 and HT1080 cells treated with increasing SAHA doses (two-way ANOVA, effect of SAHA: U87 +/+, U87 R132H/+, HT1080, $P < 0.001$; n = 3 independent experiments). **C**, Western bot of HDR factors in HT1080 cells at baseline and after radiation (6 Gy), with and without 24 hours SAHA pretreatment (5 μM) (n = 3

independent experiments). Data are represented as means ± SEM. Values below Western blot images represent relative quantification normalized to loading control.

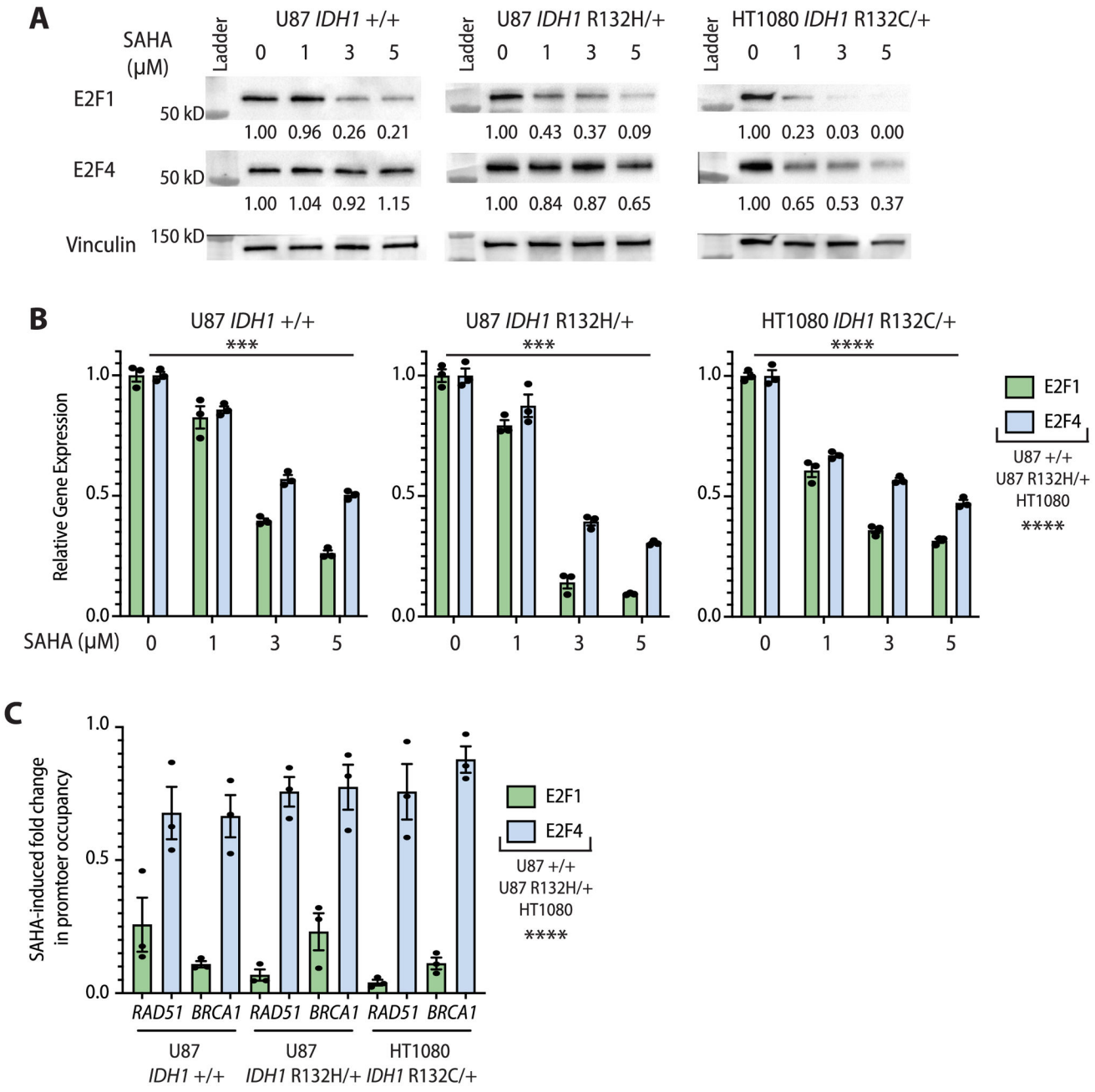

Figure 2: SAHA-induced HDR down-regulation is mediated via E2F1 loss

A, Western blot of E2F factors, E2F1 and E2F4, in U87 and HT1080 cells 24 hours after treatment with increasing SAHA doses (n = 3 independent experiments). **B**, Relative gene expression of E2F factors by RTqPCR of HDR factors in U87 and HT1080 cells 24 hours after treatment with increasing SAHA doses (two-way ANOVA, effect of SAHA: U87 +/+, U87 R132H/+, HT1080, $P < 0.001$; effect of E2F1 vs E2F4: U87 +/+, U87 R132H/+, HT1080, $P < 0.001$; n = 3 independent experiments). **C**, ChIP analysis of E2F1 and E2F4 occupancy at HDR promoters in U87 and HT1080 after 24 hours of SAHA treatment (5 μM) represented as fold change from untreated controls (two-way ANOVA, effect of E2F1 vs

E2F4: P< 0.001; n = 3 technical replicates). Data are represented as means ± SEM. Values below Western blot images represent relative quantification normalized to loading control.

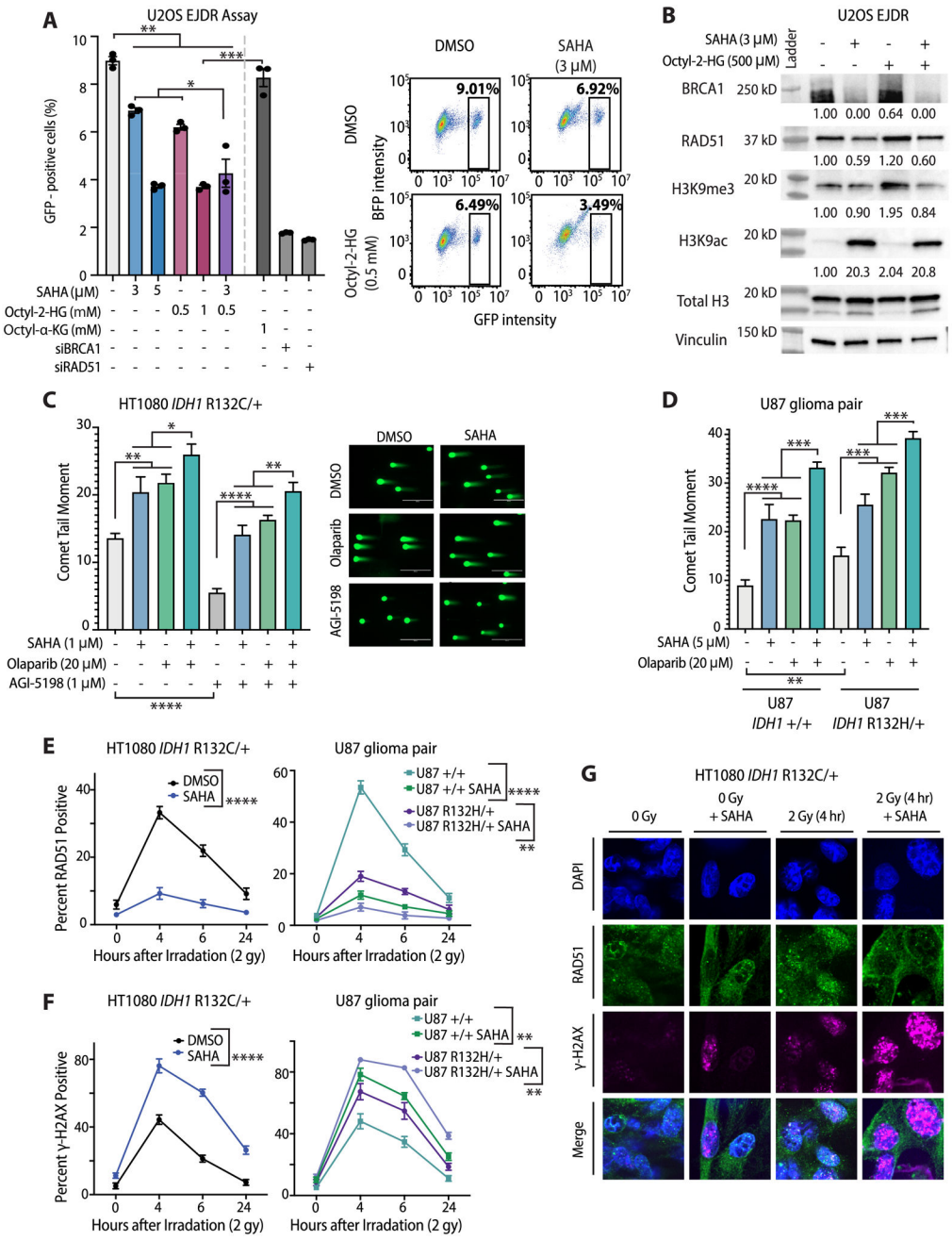

Figure 3: SAHA suppresses residual HDR in IDH1 mutant cells

A, Representative sorting and quantification of HDR via percent GFP-positive U2OS EJDR cells after treatment with DMSO, SAHA (3, 5 μM), and/or Octyl-2-HG (0.5, 1 mM), Octyl-α-KG (1mM), siBRCA1 or siRAD51 (t test, DMSO vs SAHA 3 μM, vs SAHA 5 μM, vs Octyl-2-HG 0.5 mM, vs Octyl-2-HG 1mM: P< 0.001; DSMO vs SAHA + Octyl-2-HG: P = 0.0015; SAHA 3 μM vs SAHA + Octyl-2-HG: P = 0.0118; Octyl-2-HG 0.5 mM vs SAHA+ Octyl-2-HG: P = 0.0322; SAHA 3 μM vs SAHA 5 μM, Octyl-2-HG 0.5 mM vs Octyl-2-HG 1 mM: P<0.001; SAHA 5 μM vs SAHA + Octyl-2-HG: P = 0.4083; Octyl-2-HG 1 mM vs SAHA + Octyl-2-HG: P = 0.3923; Octyl-α-KG vs Octyl-2-HG 1mM: P<0.001; DMSO vs

Octyl-α-KG: 0.1613; n = 3 biological replicates). **B**, Western blot of HDR factors, H3K9 trimethylation and acetylation in U2OS EJDR cells after SAHA and Octyl-2-HG treatment (n = 3 independent experiments). **C**, Representative images and quantification of neutral comet assays for HT1080 cells completed 24 hours after SAHA, olaparib, AGI-5198 or combined treatment (Scale bar 400 μM) (t test, DMSO vs AGI-5198: P<0.001; DMSO vs SAHA: P = 0.0011; DMSO vs olaparib: P< 0.001; SAHA vs SAHA olaparib: P = 0.042; olaparib vs SAHA olaparib: P = 0.0412; AGI-5198 vs AGI-5198 SAHA, vs AGI-5198 olaparib: P< 0.001; AGI-5198 SAHA vs AGI-5198 olaparib SAHA: P = 0.0014; AGI-5198 olaparib vs AGI-5198 olaparib SAHA: P = 0.0065). **D**, Quantification of neutral comet assays for U87 cells completed after SAHA and/or olaparib, representative images in Supplementary Fig. 3A (t test, U87 +/+ vs U87 R132H/+: P = 0.0054; DMSO vs SAHA, DMSO vs olaparib, SAHA vs SAHA olaparib, olaparib vs SAHA olaparib: U87 +/+, U87 R132H/+, P< 0.001). **E**, Percentage of RAD51 and **F**, γ-H2AX positive cells (threshold: 10 foci/nuclei) of HT1080 and U87 cells at indicated times post-irradiation (2 Gy), with or without SAHA (5 μM) (two-way ANOVA, RAD51: HT1080, U87 +/+, interaction P< 0.001; U87 R132H/+, interaction P = 0.0021; γ-H2AX: HT1080, P interaction< 0.001; U87 +/+, interaction P = 0.0013; U87 R132H/+, interaction P = 0.0087; n = 3 biological replicates). **G**, Representative images of RAD51 and γ-H2AX foci in HT1080 cells with or with SAHA, at baseline and 4 hours post-irradiation (green, RAD51; far-red, γ-H2AX; blue, DAPI; images represent 55×55 μM). Full HT1080 and U87 course in Supplementary Fig. 4A. Data are represented as means ± SEM. Values below Western blot images represent relative quantification normalized to loading control.

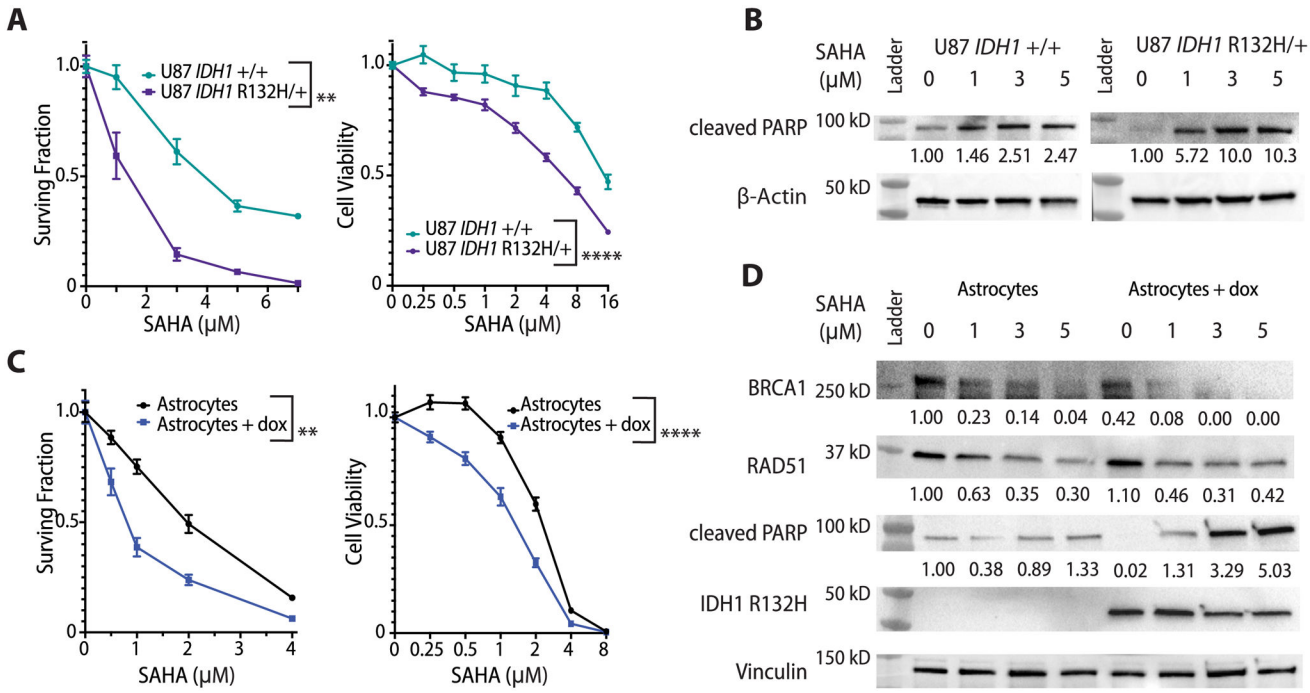

Figure 4: IDH1 mutant cells have a greater vulnerability to SAHA treatment

Clonogenic survival and cell viability, measured by ATP-based CellTiter-Glo assay, of **A**, U87 pair and **C**, IDH1 R132H-inducible M70 astrocyte line +/− dox, treated with increasing SAHA doses (two-way ANOVA, U87: survival, interaction $P = 0.0014$; viability, interaction $P < 0.001$; M70: survival, interaction $P = 0.0012$; viability, interaction $P < 0.001$; viability $n = 4$, survival $n = 3$ biological replicates). **B**, Western blot of Cleaved PARP in U87 pair after 24 hours of increasing SAHA doses ($n = 3$ independent experiments). **D**, Western blot of Cleaved PARP, HDR factors and IDH1 R132H in M70 cells +/− dox after 24 hours of increasing SAHA doses ($n = 3$ independent experiments). Data are represented as means ± SEM. Values below Western blot images represent relative quantification normalized to loading control.

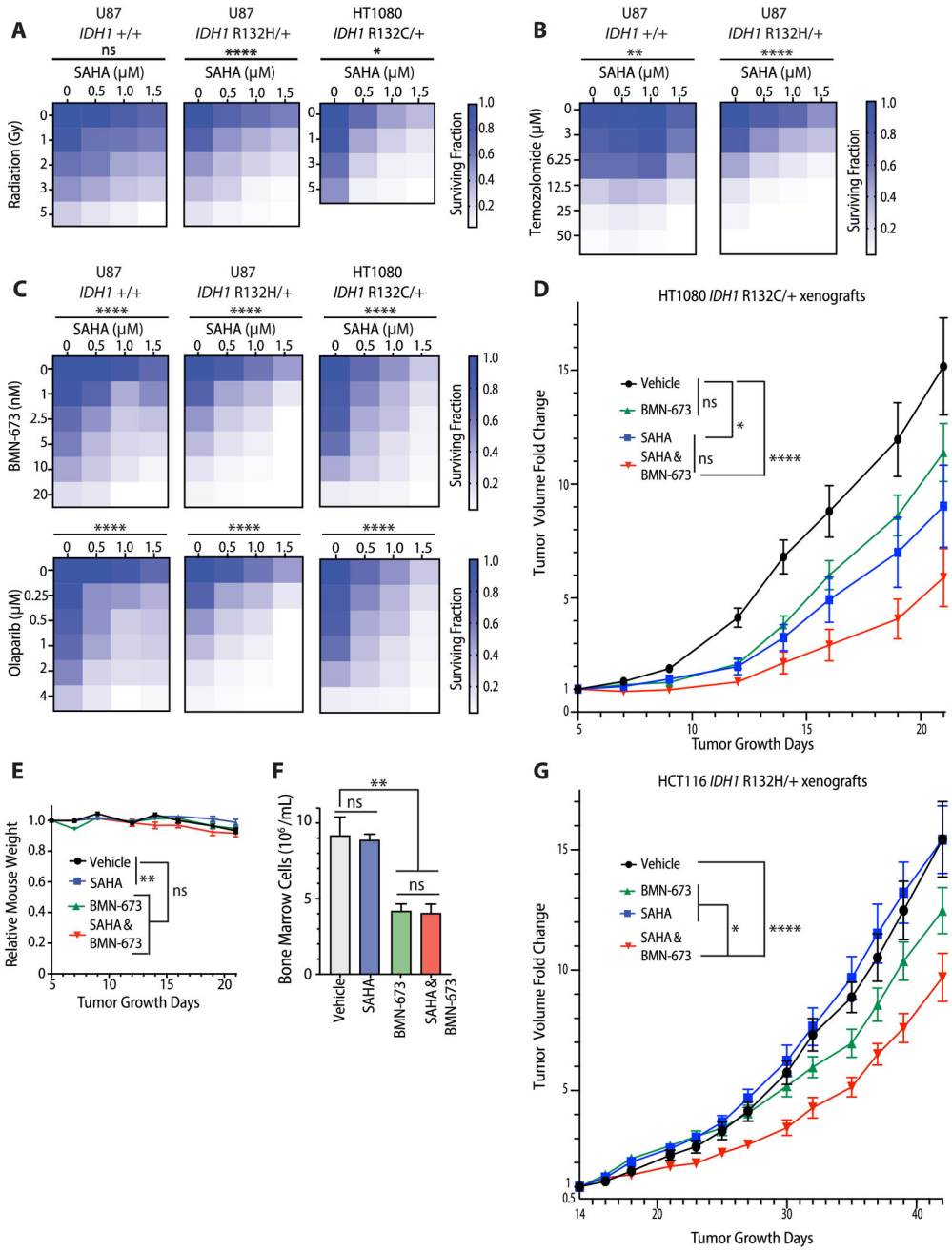

Figure 5: SAHA combination with radiation, temozolomide and PARPi is effective against IDH1 mutant cells in cell culture and tumor xenografts

Clonogenic survival of HT1080 and U87 cells treated with increasing doses of **A**, SAHA and radiation, (two-way ANOVA, HT1080, interaction P = 0.0296; U87 R132H/+, interaction P< 0.001; U87 +/+, interaction P = 0.1836; n = 3 technical replicates), **B**, SAHA and temozolomide (two-way ANOVA, U87 R132H/+, interaction P< 0.001; U87 +/+, interaction P = 0.0011; n = 3 technical replicates), **C**, SAHA and PARPi, BMN-673 and olaparib, (two-way ANOVA, BMN-673 & Olaparib: HT1080, U87 R132H/+, U87 +/+, interaction P< 0.001; n = 3 technical replicates). **D**, Growth curves of HT1080 xenograft

tumors in control mice and mice treated with SAHA (30 mg/kg) and/or BMN-673 (0.33 mg/kg) (two-way ANOVA, control vs BMN-673, interaction P = 0.1765; control vs SAHA, interaction P = 0.0132; control vs SAHA BMN-673, interaction P< 0.001; SAHA vs SAHA BMN-673, interaction P = 0.3245; n = 10 mice). Toxicity studies of SAHA, BMN-673 and combination via **E**, mouse body weight (two-way ANOVA, vehicle vs BMN-673: P = 0.0693; vehicle vs SAHA BMN-673: P = 0.1933; vehicle vs SAHA: P = 0.0142) and **F**, bone marrow cell counts (t test, vehicle vs SAHA: P = 0.8223; vehicle vs BMN-673: P = 0.0016; vehicle vs SAHA BMN-673: P = 0.0017; BMN-673 vs SAHA BMN-673: P = 0.8535). **G**, Growth curves of HCT116 IDH1 R132H/+ xenograft tumors in control mice and mice treated with SAHA (30 mg/kg) and/or BMN-673 (0.33 mg/kg) (two-way ANOVA, control vs BMN-673, interaction P = 0.0257; control vs SAHA, interaction P >0.9999; control vs SAHA BMN-673, interaction P< 0.001; SAHA vs SAHA BMN-673, interaction P< 0.001; BMN-673 vs SAHA BMN-673, interaction P = 0.0332; n = 7 mice). Data are represented as means ± SEM.